LASER INTERFEROMETER GRAVITATIONAL WAVE OBSERVATORY
- LIGO -
CALIFORNIA INSTITUTE OF TECHNOLOGY
MASSACHUSETTS INSTITUTE OF TECHNOLOGY

**Document Type T060037-00-R** February 17th, 2006

# AdLIGO HAM-SAS Mechanical Model with Lumped Elements

Valerio Boschi, Virginio Sannibale, and Riccardo de Salvo

*Distribution of this draft:*

This is an internal working note
of the LIGO Project.

California Institute of Technology
LIGO Project - MS 18-34
Pasadena, CA 91125
Phone (626) 395-2129
Fax (626) 304-9834
E-mail: info@ligo.caltech.edu

Massachusetts Institute of Technology
LIGO Project - MS 20B-145
Cambridge, MA 01239
Phone (617) 253-4824
Fax (617) 253-7014
E-mail: info@ligo.mit.edu

WWW:http//www.ligo.caltech.edu/

# 1 Introduction

This document briefly reports on the expected passive attenuation performance obtained from a dynamical model of the passive HAM-SAS system for advanced LIGO. Assumptions and approximations used in model and system dynamics are also reported, together with some discussions about extensions and improvements necessary to improve the accuracy of the model.

One of the most important feature of this model is the introduction of saturation effects due to distributed masses and the moment of inertia and counterweight. Saturations can compromise significantly the overall attenuation performance of the passive attenuation system.

The level of details achieved in this model are such that can answer the question about the fulfillment of the required attenuation performance for Advanced LIGO. Control performance, sensor and actuator characteristics, dynamics ranges, and residual RMS seismic noise will be addresses in a next document.

# 2 Mechanical Model

The HAM-SAS passive attenuation device is thoroughly described in previous documents[1]. Here we will limit our description to a level necessary to understand the simulation approximations and limits.

Let's list first the most important approximations used in the model:

- Lumped system, i.e. rigid body approximation,
- elastic elements approximated using quadratic potentials, i.e. small oscillation regime,
- dissipation mechanisms accounted using viscous damping to approximate structural/hysteretic damping,
- system assumed to be symmetric enough to separate horizontal displacements $x, y$, and yaw $\theta_z$ from pitch $\theta_y$ roll $\theta_x$ and vertical displacement $z$,
- internal modes of the mechanical structures not accounted,
- angular wires' stiffness neglected,

Using lumped system limits the accuracy of the simulation to frequency lower than the lowest internal mode. HAM-SAS is expected to have internal modes frequencies starting at around 100 Hz.

The reason of using viscous instead of hysteretic damping is because of the need of having a straightforward state space representation for time domain simulations studies. In the small oscillation regime the major difference between the two kind of damping is

that the viscous damping changes the resonant frequencies of the the modes. Practically, this turns out to be just an minor drawback because resonances are tuned to some nominal frequencies.

A symmetric system such as HAM-SAS has some orthogonal degrees of freedom that simplify the implementation of the dynamic model. Asymmetries are expected to introduce coupling no more than 1% among degrees of freedom. Therefore, for seismic attenuation performance estimation purposes such approximation should be reasonable.

Neglecting angular wires' stiffness produces an underestimation of the pendular modes frequencies, which is negligible in our case vis-a-vis the wires' cross section and tensions.

Figure 1 shows a cartoon of the mechanical model with rigid bodies, linear springs, and flexural joints. Inverted pendula counterweight bells and GASF wands and wand´ s counterweight are not shown for sake of simplicity. Due to poor graphic abilities (of the artist and not of the program used to draw) the connections of the four little pendula suspending the spring box are not shown also. More detailed sketches are shown in the two next figures.

In the model the entire mechanical system is sitting on a base which is used to excite the Attenuator in all the 6 degree of freedom. Internal resonances of the IP legs and other supporting structures are not included in the simulation.

The mechanical model has been implemented using the Maple symbolic language which produces a state space representation that can be imported into Matlab. The way that the code has been written is such that allows to progressively introduce new features to improve the accuracy and remove degrees of freedom to check the consistency of the simulation. For example, it is possible to freeze all the degrees of freedom but the one describing the IP and verify that the model gives the expected simple response similar to a compound pendulum. This feature allowed us to increase our confidence about the model.

## 2.1 GAS Filter Model

The GAS filter is modeled with an equivalent system which is able to account for most of the blades' mechanical compliances, and for attenuation saturation effects. The equivalence is achieved by tuning the model with measurements. Three orthogonal springs with the proper elastic constant are connected together by one end to the payload (the optical table), and the other three ends are attached to the filter frame. Saturation effects due to the blade's distributed mass are simulated with a wand pivoting around a point rigidly connected to the filter frame. One wand's end is then attached to a counterweight and the other is free to rotate about the point connected to the payload. The tuning of the attenuation saturation is done by changing the counterweight and/or the wand's length and/or wand's central pivot point. In the actual GAS filter wands are introduced to neutralize the attenuation saturation effects, while in the model the wands are used both to generate, end eventually to neutralize the saturations.

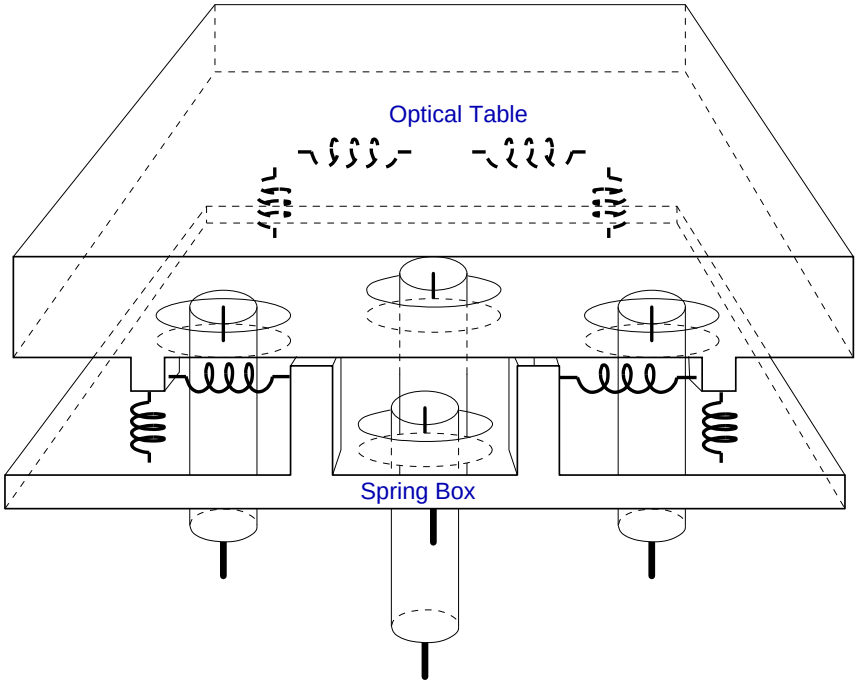


Figure 1: HAM-SAS mechanical model. The sketch does not show the connection of the four little pendula attaching the spring box to the inverted pendula , the IP counterweights, and the GAS wands and counterweight.

Figure 2 shows a sketch of the phenomenological model with two wands plus counterweight system to simulate the horizontal and vertical saturations of the transmissibility.

Figure 3 shows a comparison between a model result and measurements of the vertical transmissibility of a GAS blade with a single counterweight and wand [2]. The model has been tuned in order to match the resonance and the notch frequencies of the measurement. A significant systematic discrepancy at low frequency (below $0.2$ Hz) of approximately a 5 dB is clearly visible. The large uncertainty of the accelerometers calibration at low frequency used to take the measurement can partially explain such difference. Discrepancies above 50Hz are mainly due to the internal resonances of the supporting frame, the shaker, and the blade support designed for filter tuning studies.

## 2.2 Inverted pendulum Leg Model

The inverted pendulum dynamics have been modeled with an ideal flexural joint connected to a leg with a counterweight as shown in figure 4. The transmissibility saturation has been tuned to about -60dB, which is a conservative number considering previous measurement with the HAM-SAS IP legs. IP Resonant frequency was tuned to 30 mHz, which is a frequency routinely obtained by Virgo super-attenuators and also obtained by

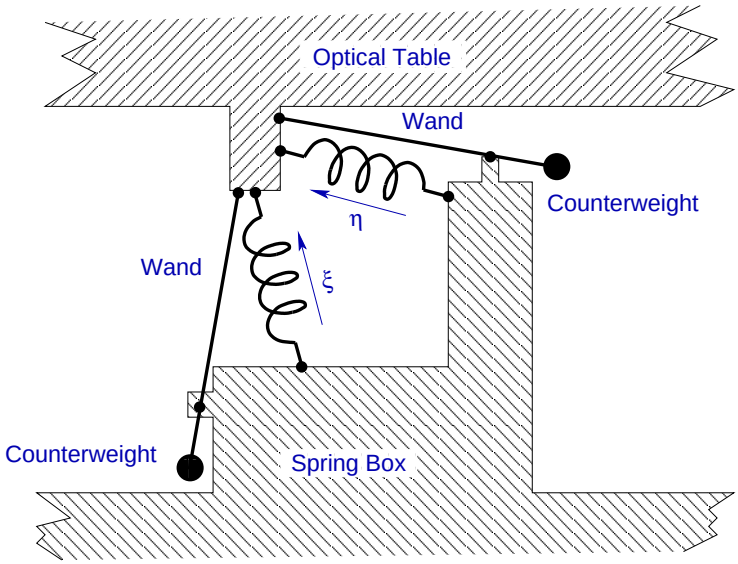


Figure 2: GAS filter model sketch. The third spring and the third wand+counterweight are not shown because are orthogonal to the drawing. Pivot points are shown with black dots.

SAS prototypes.

## 2.3 Simulation Parameters

For this preliminary study we have considered the system symmetric, i.e. each GAS and each inverted pendulum are described by the same parameters. The following table shows the parameters used in the simulation.

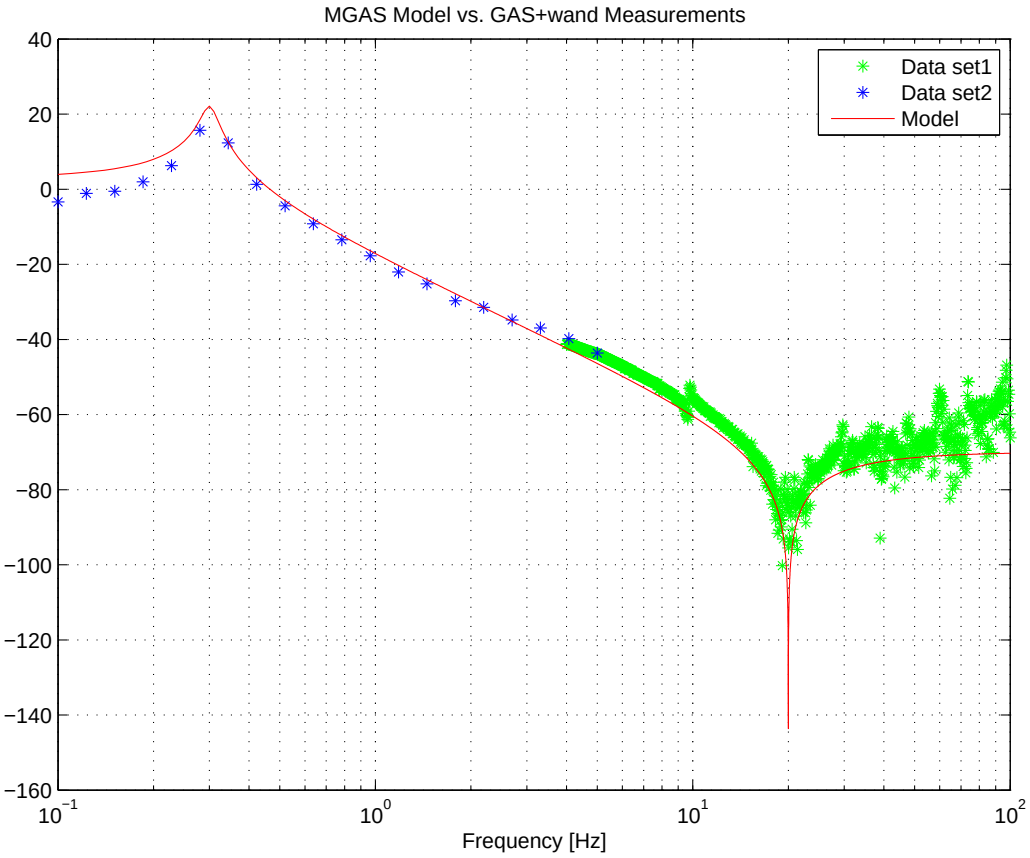


Figure 3: Comparison of modeled and experimental vertical transmissibility of an GAS filter with assembled with a wand with a counterweight. Experimental data were taken in two separate measurements [2]: green asterisks Data set #1, blue asterisks Dataset #2.

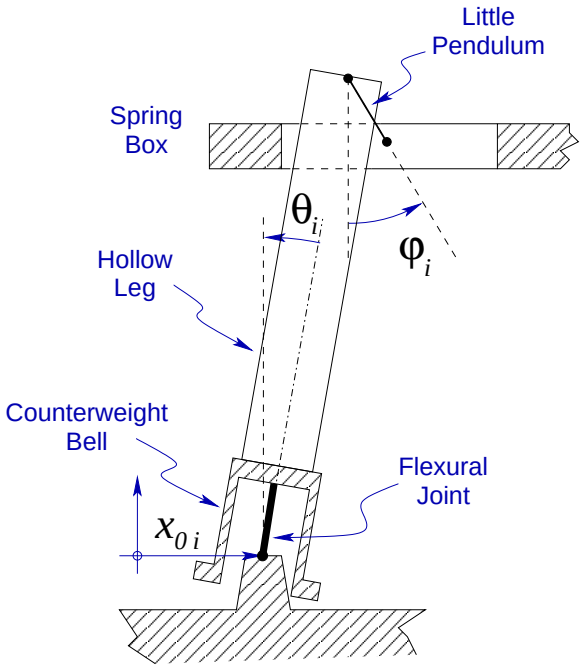


Figure 4: Inverted pendulum mechanical model sketch. Pivoting point are shown with black dots. The connection between the spring box and the little pendulum is not clear from the sketch.

| Parameter | Value |
|---|---|
| GAS Vertical resonance frequency | 0.03 Hz |
| GAS Vertical notch frequency | 20 Hz |
| Measured GAS horizontal resonance frequency | 0.54 Hz |
| GAS horizontal notch frequency | 20 Hz |
| Distance between Vertical wand's pivoting point and counterweight | 0.238 m |
| Distance between Horizontal wand's pivoting point and counterweight | 0.242 m |
| Wands counterweight masses | 0.1kg |
| Distance between GAS along $\hat{x}$ axis, and $\hat{y}$ axis | 1.1 m, 0.9 m |
| Inverted pendulum (IP) resonance frequency | 0.05 Hz |
| IP total length | 0.685 m |
| IP total mass | 2.858 kg |
| Position of the IP leg center of mass | 0.534 m |
| Upper small flex joint length | 0.030 m |
| Distance between IP legs along $\hat{x}$ and $\hat{y}$ axes | 0.1 m, 1.105 m |
| $xx$ component of the IP leg inertia tensor | 0.061 kg m$^2$ |
| $yy$ component of the IP leg inertia tensor | 0.061 kg m$^2$ |
| $zz$ component of the IP leg inertia tensor | 0.130 kg m$^2$ |
| Mass of the optical table | 906 kg |
| $xx$ component of the optical table inertia tensor | 254.3 kg m$^2$ |
| $yy$ component of the optical table inertia tensor | 531.6 kg m$^2$ |
| $zz$ component of the optical table inertia tensor | 306.0 kg m$^2$ |
| Mass of the spring box | 250 kg |
| $zz$ component of the spring box inertia tensor | 200 kg m$^2$ |

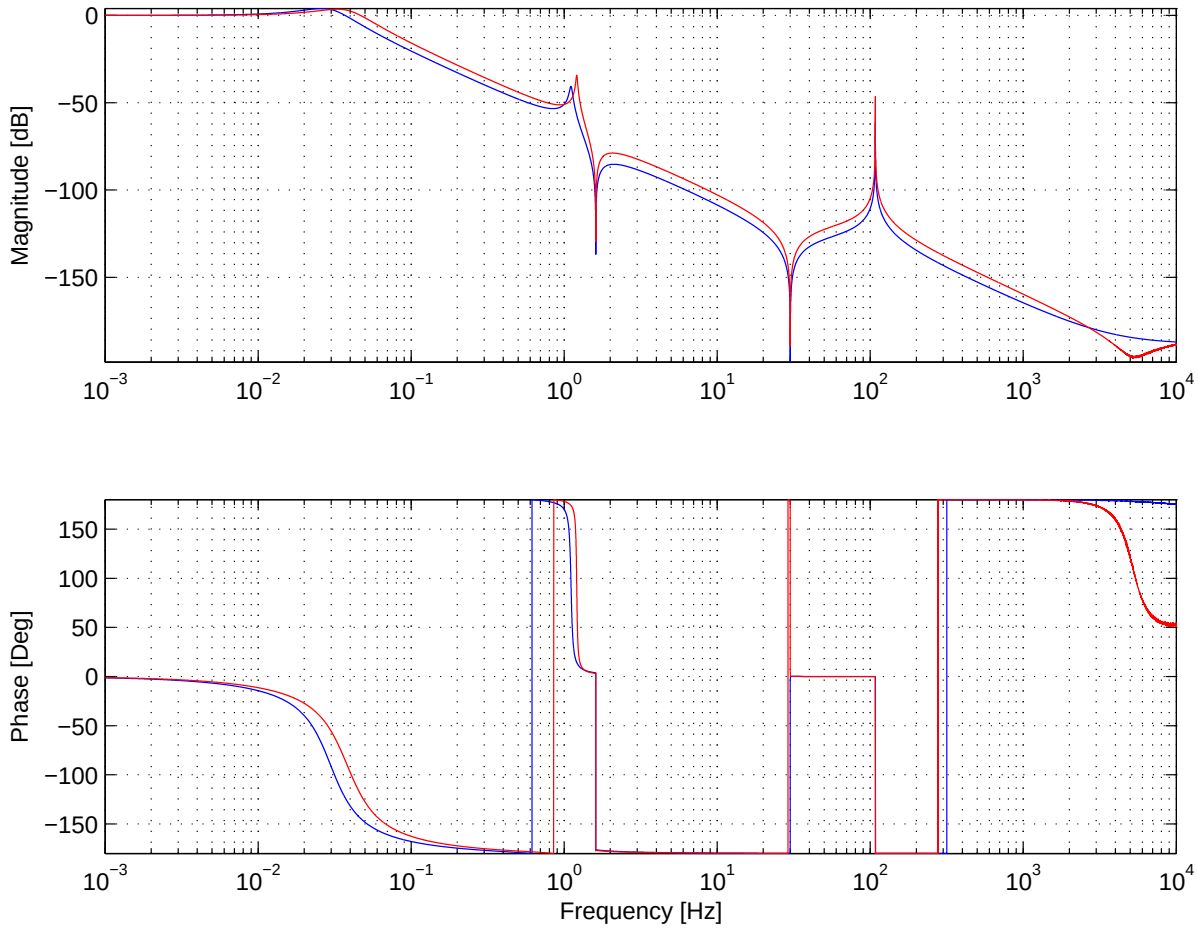


Figure 5: Transmissibility for the horizontal (blue) and yaw (red) degree of freedom. The 103Hz quality factor was left to $\infty$.

# 3 Transmissibilities

Transmissibilities from ground to the optical table center of mass for all the six degrees of freedom are shown in the next pages. To compute such transmissibilities we first calculate the transfer functions from generalized forces (forces or torques) applied to the shaker base to the optical table degrees of freedom. Then the transmissibilities are been obtained applying the proper transfer function ratios to remove the dependency on the generalized forces. Because internal modes are not included in the mechanical models this simulation have to be considered "cum grano salis", i.e. they are valid up to approximately 50 Hz. Above that frequencies discrepancies are expected to be large especially around the internal mode frequencies. Distributed masses increase broadly the difference.

### $x_0$ to $x$ transmissibility

The blue curves of Figure 5 are the transmissibility of the horizontal degree of freedom $x$. The resonance at 30 mHz with very low quality factor corresponds to the inverted pendulum mode frequency. The 1.2Hz resonance is due to the horizontal stiffness of the GASF blades, which has been experimentally measured to be about 0.54 Hz using a GAS filter prototype. Finally, the resonance at 103 Hz is due to the short pendula which connect the inverted pendulum legs to the GASF frame. Saturation above 2 Hz has been tuned using the inverted pendulum counter-weight to about -65 dB, which is considered a reasonable value after the past Virgo results and measurements on HAM-SAS legs.

### $y_0$ to $y$ transmissibility

Because of the symmetry of the system, the transmissibility curves for the horizontal degree of freedom $y$ is essentially the same as the $x$ degree of freedom. Minor differences come from the moments of inertia and lever arms which are differ by less than 10% in the two orthogonal directions.

### $\theta_z^{(0)}$ to $\theta_z$ transmissibility

The red curves of Figure 5 show the transmissibility for the angular degree of freedom $\theta_z$ (yaw).

### Vertical $z_0$ to $z$ transmissibility

The blue traces of Figure 6 are magnitude and phase of the transmissibility of the vertical degree of freedom $z$ . The vertical resonance has been tuned at 30 mHz and the saturation has been set to about -60dB. Those values have been experimentally obtained for a GASF with a payload of about the same of the HAM-SAS system. Saturation can be lowered by several dB using a properly tuned wand and counterweight. The major advantage in lowering the saturation levels is to reduce the magnitude of the internal resonances in the transmissibility curves. The quality factor for the vertical resonance was set to about 3.

### Roll $\theta_x^{(0)}$ to $\theta_x$ transmissibility

The red traces of Figure 6 are magnitude and phase of the transmissibility of the angular degree of freedom $\theta_x$ (roll). As expected this transfer function is similar to the vertical transfer function but with different resonant frequency( this resonance depends on the moment of inertia of the payload and not just on the mass )

### Pitch $\theta_y^{(0)}$ to $\theta_y$ transmissibility

The green traces of Figure 6 are magnitude and phase of the transmissibility of the angular degree of freedom $\theta_y$ (pitch). The different between the previous transmissibility is mainly

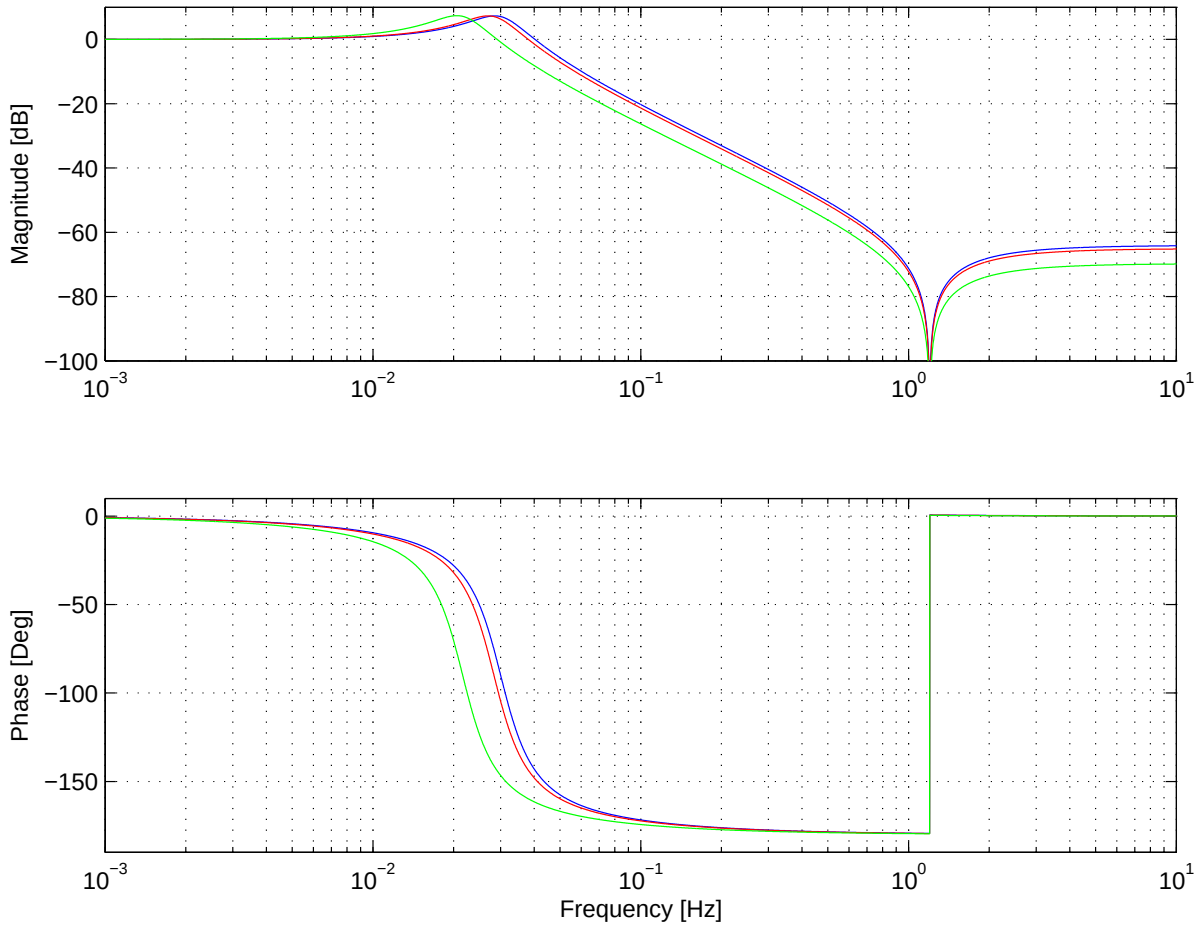


Figure 6: Transmissibility for the vertical (blue) , pitch (red) and roll (blue) degrees of freedom.

due to the different moment of inertia about the $x$ and $y$ axis.

# 4 Seismic Noise Models

The Seismic noise reference spectra used to estimated the attenuation of the horizontal and vertical seismic spectra were taken from the AdLIGO requirement document[3], which horizontal and vertical reference spectra to be the same but one for each site. The seismic noise reference spectrum used in the simulation is the envelope of LLO and LHO reference spectra from 100mHz to 40 Hz. Below 100mHz those reference spectra have been extrapolated using Peterson's New Low Noise Model [4]. The ground tilt noise was generated in the 10 mHz - 40 Hz band using the Rayleigh waves propagation model[5]. Such model is probably not very accurate to describe the actual noise of the LIGO sites

especially because of asymmetries and of the internal modes of the HAM supporting structure at low frequencies which introduce phase delays in the noise propagation. Direct measurements are needed to estimate the amount of angular noise.

# 5 Attenuation Performance

### $x_0$ to $x$ power spectrum

Figure 7 shows the reference spectrum, the design requirement spectrum and two predicted attenuated spectrum for the horizontal degree of freedom. The blue curve is considering the inverted pendulum resonant frequency tuned at 20 mHz and the red curve with the IP tuned at 30mHz. The red curve shows that requirements cannot be met in the 0.8-1.5Hz interval. The blue curve shows a better attenuation of the low peak. In the conclusion section, with a 30mHz IP tune, we briefly resume possible solutions of such problem.

### $y_0$ to $y$ power spectrum

The filtered seismic noise spectrum for the horizontal degree of freedom $y$ is not reported because is essentially the same as the $x$ horizontal degree of freedom. In fact the only differences comes from a slight difference on the two horizontal transmissibilities.

### $z_0$ to $z$ power spectrum

Figure 8 shows the filtered and unfiltered power spectral density of the vertical degree of freedom $z$ . Requirements are met everywhere with a saturation of the about -60dB which is a value that has been easily reached experimentally without using counterweighted wands.

### $\theta_x^{(0)}$ to $\theta_x$ Power Spectrum

Figure 9 shows the filtered and unfiltered power spectral density of the the angular degree of freedom $\theta_x$ (roll). Requirements are met met everywhere with a quite large safety margin. Because the arm lever of the triple pendulum supporting frame is about 1m long the angular noise translates directly into meters. It is important to mention that the ground angular noise spectrum is probably underestimated.

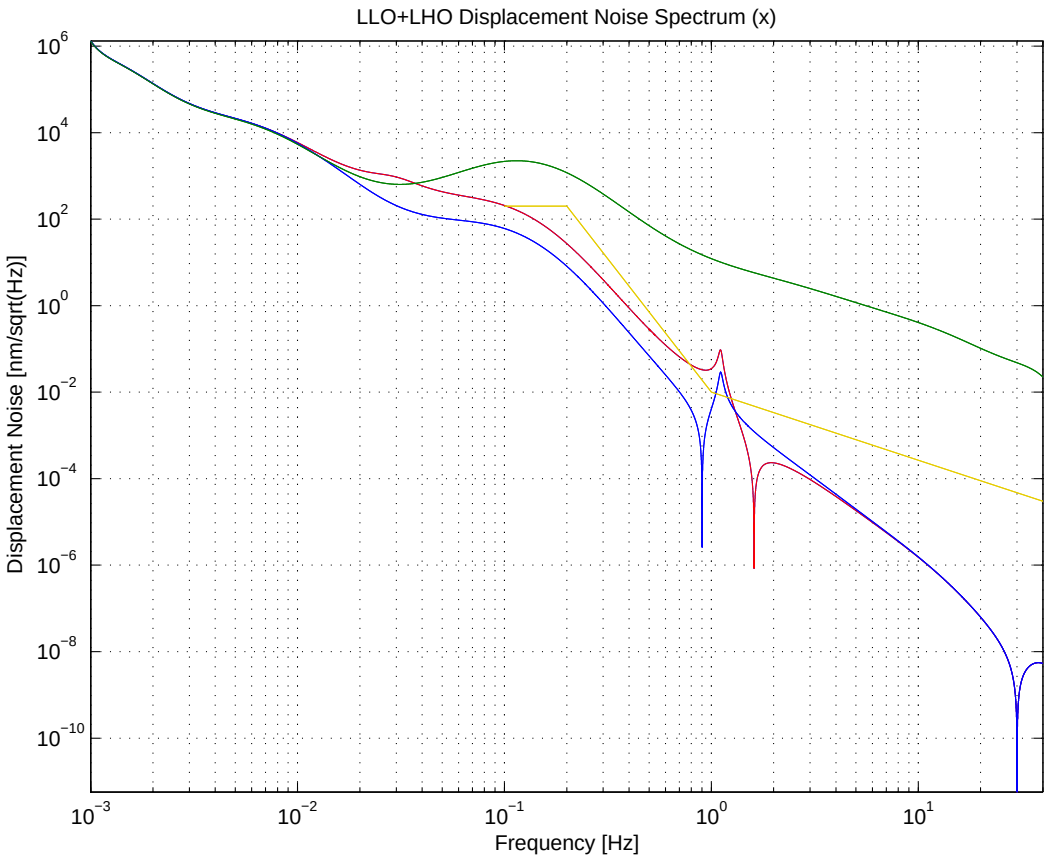


Figure 7: Seismic noise square-root power spectral densities of the horizontal ($x$) degree of freedom: gold curve AdLIGO noise requirements, green curve seismic noise reference, blue and red curve filtered seismic noise with IPs tuned respectively to 30 mHz and 20 mHz.

### $\theta_y^{(0)}$ to $\theta_y$ power spectrum

The filtered seismic noise spectrum for the angular degree of freedom $\theta_y$ is not reported because is essentially the same as the roll $\theta_x$

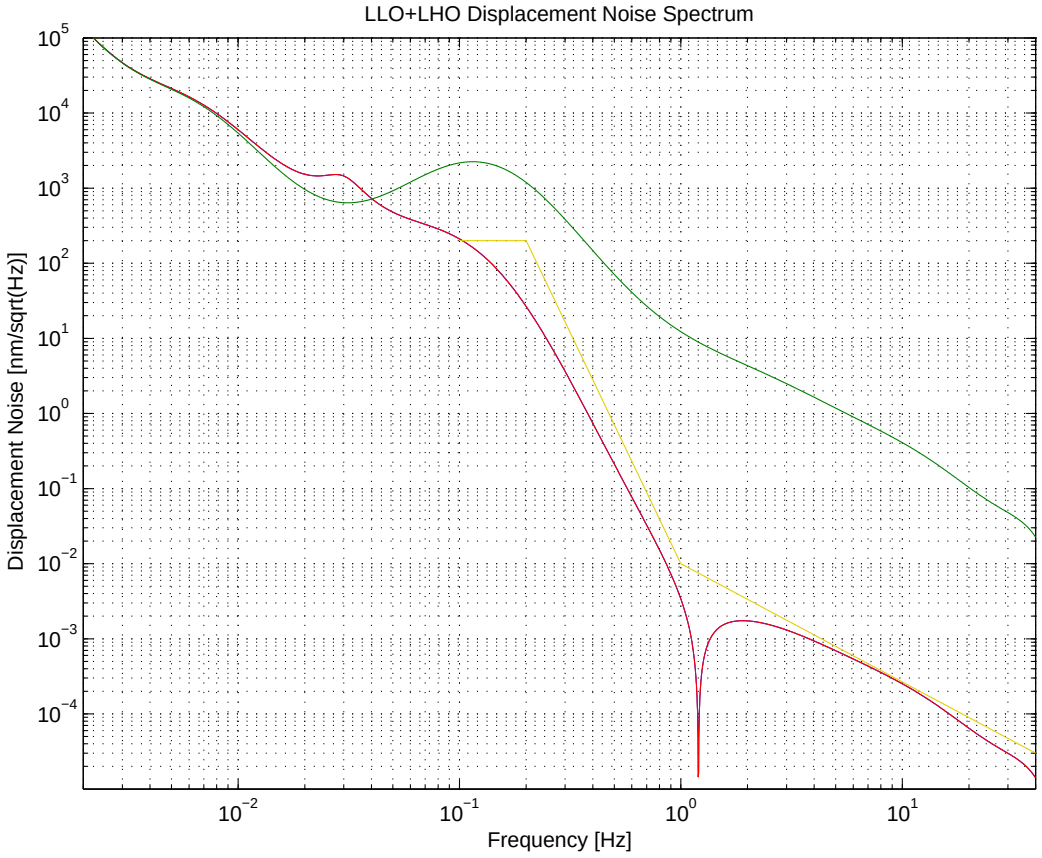


Figure 8: Seismic noise square-root power spectral densities of the vertical ($z$) degree of freedom: light green curve required Ad LIGO noise performance, dark green curve seismic noise model, and red curve filtered seismic noise.

### $\theta_z^{(0)}$ to $\theta_z$ power spectrum

Finally Figure 11 shows the filtered and unfiltered power spectral density of the angular degree of freedom $\theta_z$ (yaw). Requirements are met everywhere with a quite large safety margin. As in the other angular degrees of freedom, the angular noise roughly translates into position noise expressed in meters. It is important to mention that the angular noise spectrum is probably underestimated.

# 6 Conclusion

Results from this simulation looks quite promising. The predicted attenuation performance are met with a large margin above 2Hz and below 200 mHz with a good safety margin. Because of the horizontal stiffness of the GAS filter between 0.2 Hz to 2 Hz the

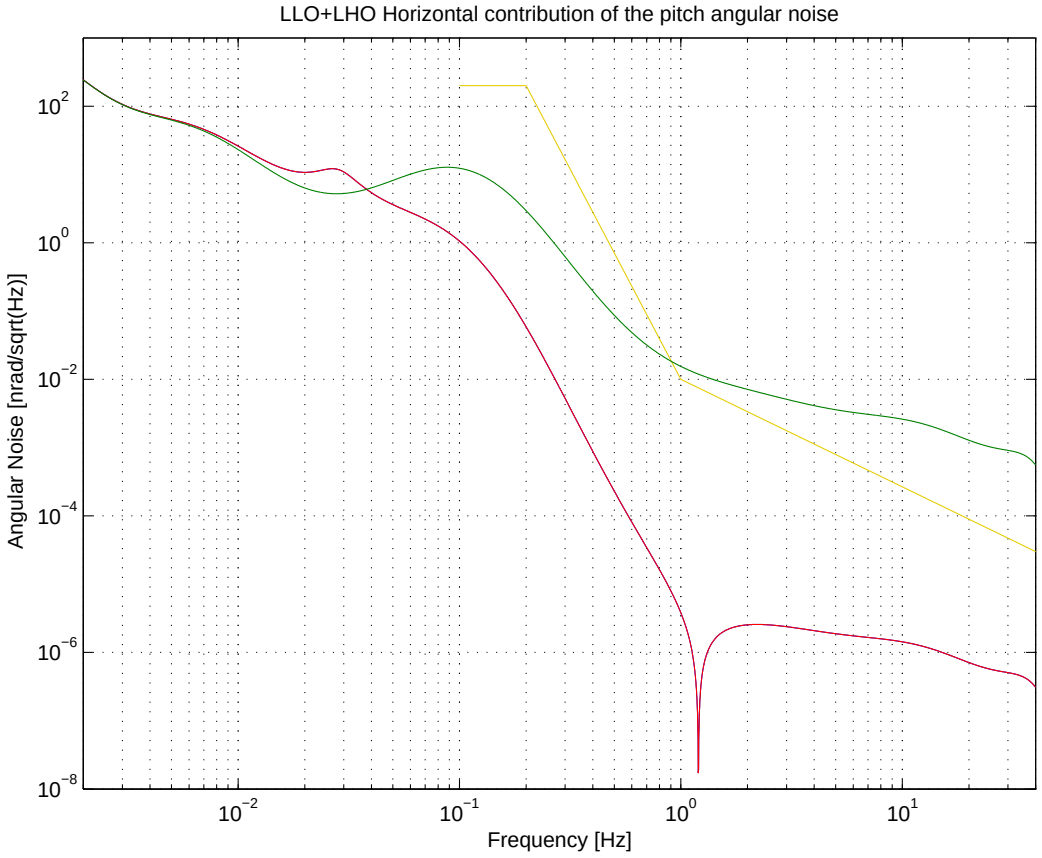


Figure 9: Seismic noise square-root power spectral densities of the horizontal ($\theta_x$) degree of freedom: gold curve is the required AdLIGO noise performance, green curve is seismic noise model, and the red curve is filtered seismic noise.

requirement may not completely met by a factor 2 or less on average.

Several remedies are possible to fix such issue, and they can even be combined together. The most elegant way is to tune the notch produced by the inverted pendula counterweight at the GAS resonant frequency to add passive attenuation in correspondence of that GAS horizontal resonance.

A second possibility is to tune the inverted pendulum resonant frequency below 30mHz down to 20mHz to substantially lower the 1.2 Hz resonance.

Fifth but not least, one can apply an active control such as inertial damping or local relative viscous damping to reduce the height of the resonance. Space is foreseen in the spring box for sensors and actuators dedicated to this task. These instruments would work in the horizontal direction inside the spring box, orthogonally to its main oscillation degrees of freedom, and therefore will not degrade its performance.

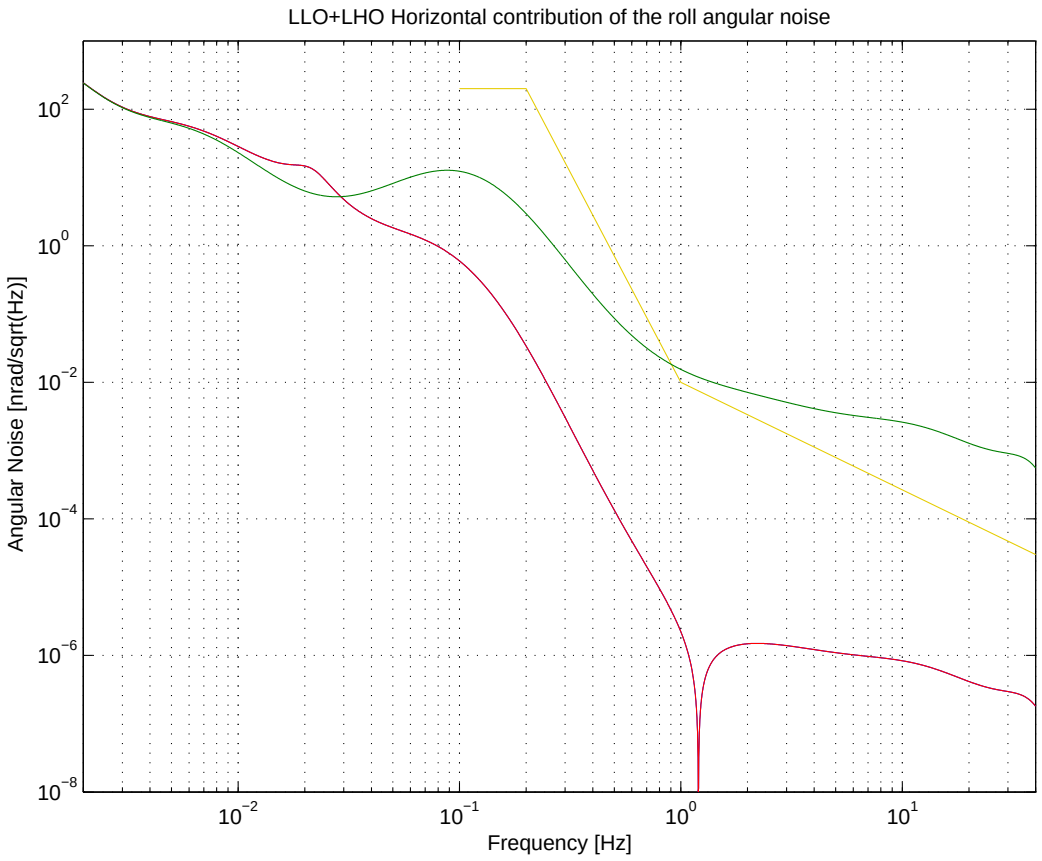


Figure 10: Seismic noise square-root power spectral densities of the horizontal ($\theta_y$) degree of freedom: gold curve required AdLIGO noise performance, green curve seismic noise model, and red curve filtered seismic noise.

# 7 Further Developments

A very simple step to improve the model is to introduce the missing vertical mode of the four little pendula, and their angular stiffness .

The next steps to improve the model is to progressively introduce some asymmetries to study tolerances on alignments and on the fabrication of specific parts.

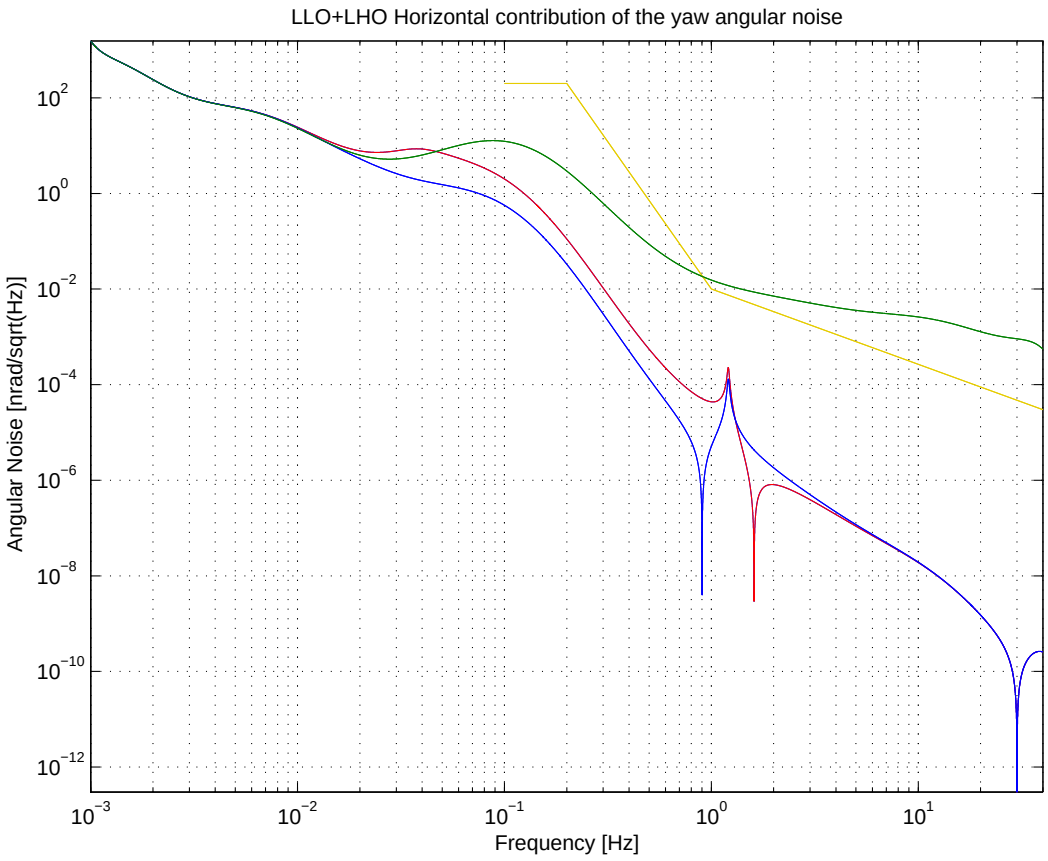


Figure 11: Seismic noise square-root power spectral densities of the horizontal ($\theta_z$) degree of freedom: gold curve required AdLIGO noise performance, green curve seismic noise model, blue and red curve filtered seismic noise for a system with IPs tuned respectively at 30 mHz and 20 mHz.

# References


[1] A.Bertolini et al., *Design and prototype tests of a Seismic Attenuation System for the Ad-LIGO Output Mode Cleaner*, P050024-00-D

[2] A. Stochino and R. de Salvo, *Performance Improvement of the Geometric Anti-Spring (GAS) Seismic Filter for Gravitational Wave Detectors*, SURF Report, T050239-00.

[3] LIGO Systems, Ed. D. Shoemaker, *The LIGO Observatory Environment*, T010074-03

[4] J. Peterson, *Observation and modeling of seismic background noise*, U.S. Geol. Surv. Tech. Rept., 93-322, 1-95, 1993

[5] A.Takamori, *Low Frequency Seismic Isolation for Gravitational Wave Detector*s, Ph.D. thesis, P030049-00.